

# Carbon CO<sub>2</sub> Reuse in Direct DME Synthesis from Syngas

EURECHA Student Contest Problem Competition 2017

Alba Carrero Parreño, Juan Diego Medrano García, Natalia Quirante

Institute of Chemical Processes Engineering, University of Alicante, PO 99, E-03080 Alicante, Spain

## Abstract

---

In this work, we propose a process to reduce CO<sub>2</sub> emissions through its capture and utilization (CCU) as a raw material for producing valuable products in the chemical industry. As a case study, we design and evaluate the economic and environmental performances of a direct dimethyl ether (DME) synthesis from syngas plant reusing CO<sub>2</sub> as a raw material. The decision making is carried out including all the design variables into a flowsheet superstructure, which is simulated and optimized to maximize the process profit. The optimum production of DME is 219.95 kt/year at 99.95% purity, with a profit of \$51.01 million/year and emitting 0.784 kg CO<sub>2</sub>-eq/kg DME produced. After heat integration implementation, the profit is raised to \$58.68 million/year and emissions are reduced to 0.510 kg CO<sub>2</sub>-eq/kg DME, being the latter a 61.4% lower than the one associated to the classic DME production. The financial risk associated with the post heat integration process is at 15.4%, while considering a 5% risk decreases this value to \$40.25 million/year.

---

## 1 Preliminary study

As the global warming concern rises among people, carbon capture and storage (CCS) techniques have been developed to lessen the impact of carbon dioxide emissions. However, as the last stage of these methods (i.e., the storage) is just a way of literally burying the problem, the carbon capture and utilization (CCU) concept has emerged in order to truly get rid –and meantime take advantage– of the captured CO<sub>2</sub>. This reuse of CO<sub>2</sub> diverges into two different paths: the indirect and the direct route. In the first, the gas is used per se (in the food industry as an additive, packaging gas or extraction fluid; in addition, to dry cleaning, fire extinction, water treatment or respiratory stimulation). In the second, it is converted into valuable chemicals.<sup>1</sup> Hence, the direct conversion route stands out as a more definitive way to solve the CO<sub>2</sub> problem.

Urea, inorganic carbonates, and methanol production processes comprise about 200 Mt/y of CO<sub>2</sub> consumed in the chemical industry.<sup>2</sup> These processes are well-known and their CO<sub>2</sub> sources used (e.g., ammonia synthesis for urea) already established. Thus, developing alternative technologies for already existing non-CO<sub>2</sub>-consuming processes is the key to further extend the CO<sub>2</sub> utilization in the chemical industry. A couple of chemicals that fall into this category are ethanol and dimethyl ether, and as an even less conventional alternative technology, photocatalytic reduction of CO<sub>2</sub>.

Ethanol is produced mainly via fermentation (sugar cane, maize, potatoes, rye, sugar beet, whey, sorghum, etc.) and to lesser extent by hydration of ethylene to produce industrial grade pure ethanol.<sup>3,4</sup> However, glucose fermentation (be it aerobic or anaerobic) directly emits CO<sub>2</sub> as a byproduct. Alternatively, ethanol production from syngas has been studied since the discovery of the Fischer-Tropsch synthesis reaction.<sup>3</sup> A synthesis by homogenous catalysts has been reported to have high selectivity in contrast to an expensive separation of the product ethanol from the catalyst. On the other hand, a synthesis by heterogeneous catalysts eases the separation but achieves low selectivity.<sup>4</sup> Both processes are still under development in order to improve their capabilities. In addition, as an even more promising process, ethanol has been synthesized via direct electrolysis of CO<sub>2</sub> in water with 83% selectivity at ambient temperature and pressure and without the need of an expensive noble metal catalyst.<sup>5</sup> This finding makes the future of ethanol as a fuel much brighter, although due to the recent novelty of the discovery, few data is available, thus, not allowing a proper study of the process to date.

Dimethyl ether (DME) was –and still is– traditionally made from methanol in a two-step synthesis. Even though it is well known that methanol can be synthesized using a CO<sub>2</sub>-rich syngas, doing so increases the production cost.<sup>1</sup> Alternatively, a new process in which DME is produced directly from

syngas was developed in the past years.<sup>3</sup> Although this technology produces CO<sub>2</sub> as a byproduct, the syngas feed for the synthesis requires an H<sub>2</sub>/CO ratio of one. A close enough ratio can be achieved throughout dry methane reforming (DMR), in which methane and CO<sub>2</sub> react to produce syngas. A recent study claims that at 100 kPa, 850 °C, 1:1 CH<sub>4</sub>/CO<sub>2</sub> inlet ratio with a Pt + Ni-based catalyst, an equilibrium conversion is achieved avoiding carbon deposition problems at high reaction times.<sup>6</sup> Based on these facts, a ~97% of the fed CO<sub>2</sub> is converted to obtain a syngas with an H<sub>2</sub>/CO ratio of 0.968. Using this syngas as synthesized and deducting the CO<sub>2</sub> produced in the DME reaction, a consumption of 0.669 kg CO<sub>2</sub>/kg DME is achieved. In contrast, the classic process releases a net emission of 1.321 kg CO<sub>2</sub>-eq/kg DME.<sup>7</sup> Although unlike the first, the latter value also takes into account the GWP (a LCIA method) values for utilities and raw materials, these results seem to make worthwhile a more detailed study of the DME process.

The photocatalytic (PC) reduction of CO<sub>2</sub>—commonly branded as artificial photosynthesis of CO<sub>2</sub>— is a technique in which CO<sub>2</sub> and H<sub>2</sub>O react with the aid of a photosensitive catalyst under a source of light to form hydrocarbon fuels and O<sub>2</sub>.<sup>8</sup> The final products (e.g., methane, methanol, formaldehyde, formic acid, etc.) depend on the correlation of the energy levels of the semiconductor and the redox agents,<sup>9</sup> thus conforming a wide array of possibilities. Even though significant advances have been made in the PC reduction of CO<sub>2</sub>, conversion efficiency and selectivity are to be significantly improved for this process to see an actual industrial implementation,<sup>9</sup> which will suppose a revolution in the energy sector.

We have chosen DME among the three options since there is more data available to develop a more detailed study. Furthermore, DME is an environmentally friendly chemical since it can substitute ozone layer damaging aerosol propellants and coolants, can be used effectively in diesel engines reducing NO<sub>x</sub>, particles and noise during the combustion, as pesticide, polishing and anti-rust agent and as intermediate in the synthesis of ethylene, propylene, gasoline, oxygenates, acetaldehyde, acetic acid, etc.<sup>10,11</sup>

## 2 Process design overview

The DME synthesis plant will be located near a source of CO<sub>2</sub>. A natural gas combined cycle power plant with a capacity of 770 MW and an emission of 1.7 Mt/y of CO<sub>2</sub> has been chosen for this task.<sup>12</sup> The CO<sub>2</sub> capture is carried out with 48 wt% diglycolamine (DGA) in a 20 stage absorber column and a 7 stage stripper column with 26 m<sup>3</sup>/h solvent circulation rate, 1903 kW of reboiler duty with a total cost of \$43.06/t of CO<sub>2</sub>.<sup>13</sup> The production of DME can be divided into four stages: syngas production, compression system, DME production, and product separation. In each stage, we proposed different alternatives which will be described in the following subsections. Figure 1 shows the superstructure of the DME production process .

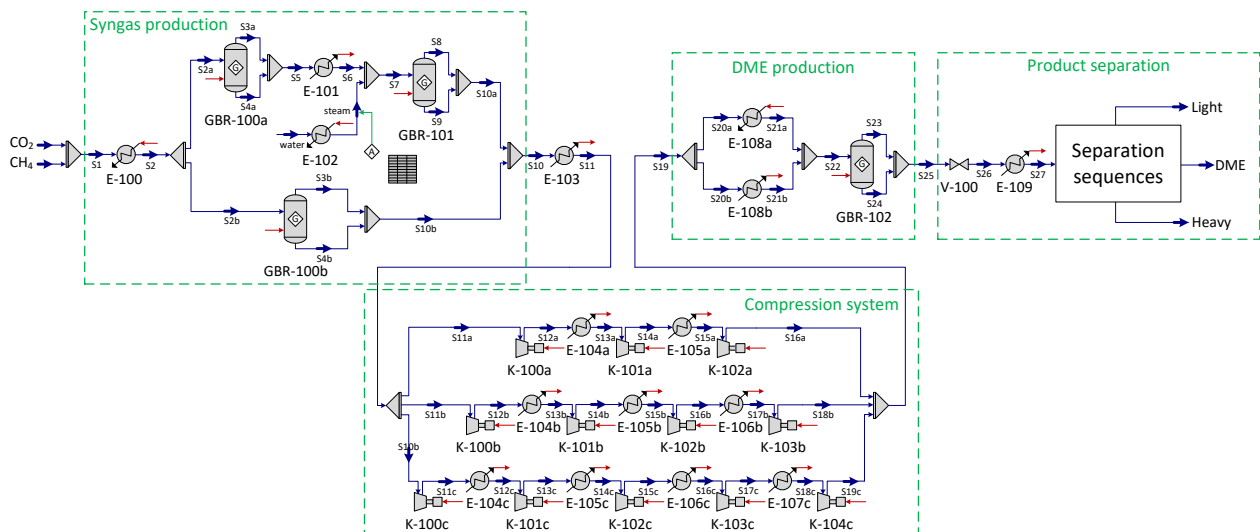
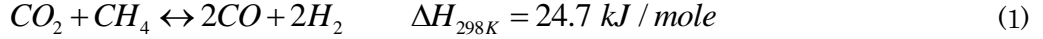


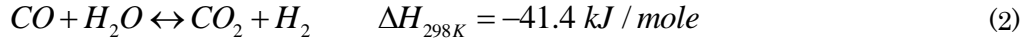
Figure 1. Superstructure of the DME production process.

## 2.1 Syngas production: dry methane reforming and water gas shift reaction

The main reaction of the system to produce DME requires syngas as a raw material. Syngas can be obtained using several technologies, including steam methane reforming (SMR), catalytic and non-catalytic partial oxidation (CPO, POX), autothermal reforming (ATR), dry methane reforming (DMR), bi-reforming (BR) and tri-reforming (TR).<sup>3,14-17</sup> These processes employ a reforming agent (steam, oxygen, CO<sub>2</sub> or mixtures) and generally methane at high temperatures to produce the syngas. Due to the different operation pressures and temperatures and reforming agents required in each process, the final syngas composition (H<sub>2</sub>/CO ratio) varies significantly. For DME synthesis, a ratio of 1 has been proven optimum for the reaction.<sup>11</sup> The process which supplies a closer ratio to the desired one is DMR (100 kPa, 850 °C, 1:1 methane/CO<sub>2</sub>), which on top of that consumes CO<sub>2</sub>.



However, the obtained ratio is slightly below 1. To adjust the value, a water gas shift (WGS) reactor can be used. The water gas shift reaction consists in the equilibrium reaction of CO and steam (favored at low temperatures) and CO<sub>2</sub> and H<sub>2</sub> (favored at high temperatures). Thus, lowering the temperature (250 °C) and through the addition of steam, some of the excess CO can be turned into H<sub>2</sub>, although generating CO<sub>2</sub> in the process.



We consider that the natural gas employed as a raw material consists of 100% methane. Commercial natural gas usually contains approximately 95-96% of methane,<sup>7,18</sup> inert nitrogen that does not affect the reactions; and ethane, propane and other hydrocarbon traces contained in the mixture which are more than likely to be reformed along with the methane. Captured CO<sub>2</sub> from the power plant is considered pure as well. We used Gibbs equilibrium reactors in Aspen HYSYS to simulate the reactors. The final syngas with an H<sub>2</sub>/CO ratio of 1 (considering the WGS reactor [GBR-100a and GBR-101]) or less (no considering the WGS reactor [GBR-100b]) is then sent to the compression stage.

## 2.2 Compression system optimization model

The direct synthesis of DME requires the pressurization of the produced syngas. Previous studies<sup>19</sup> demonstrate that working in an operative range of 4000-9000 kPa leads to minor variation in the syngas conversion (i.e., 7900 kPa (91%) and at 4000 kPa (86%)) with the non-significant impact of methanol co-produced. In this regard, it should be noted that working at higher pressure also increases the duty required.

The number of compression stages can be estimated from heuristics for compressors. In general, the maximum compression ratio is taken to be around four.<sup>20</sup> The following expression determines the compression ratio  $r$  for minimum work and  $N$  stages:

$$r = \sqrt[N]{\frac{P_{OUT}}{P_{IN}}} \quad (3)$$

where  $P_{OUT}$  and  $P_{IN}$  are, respectively, the outlet and the inlet pressures of the compression system. Table 1 shows the compression ratio calculated from Eq.(3) for our system composed of one to five stages at different outlet pressures and at  $P_{IN} = 100$  kPa. By considering that the maximum compression ratio should be around four, we can expect the optimum number of compression stages to be three, four or five.

Table 1. Compression ratio as a function of number of stages and outlet pressure.

Number of stages	1	2	3	4	5
P <sub>OUT</sub> (kPa)	Compression ratio				
6000	60	8	4	3	2
7000	70	8	4	3	2
8000	90	9	4	3	2

Figure 2 shows the proposed superstructure for carrying out the optimization of the compression system.

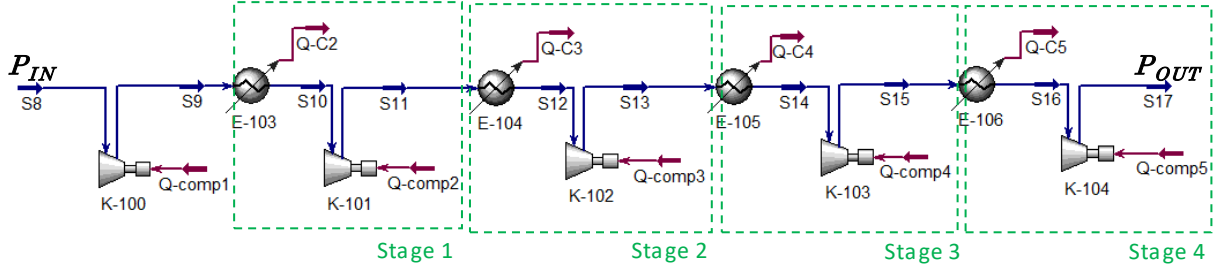


Figure 2. Compression system superstructure.

The model has the following continuous and binary variables:

- Continuous variables include the compression ratio for each compressor ( $r_0$  for compressor one, which always exists, and  $r_i$  for each conditional compressor) and the outlet temperature for each intercooler ( $T_i$ ). The low dew point of the working fluid removes the risk of having condensates in the pipeline. Therefore, the cooler's outlet temperature has been limited to an operative range of (-100 – 150 °C) using different refrigerant fluids.
- Binary variables represent the discrete decision concerning with the existence or not of each compressor stage (intercooler and compressor).

Using the Generalized Disjunctive Programming (GDP)<sup>21,22</sup> approach, which uses higher level of logic constructs that make the formulation step more intuitive, the optimization problem can be formulated as follows:

$$\begin{aligned}
 \min \quad & TAC_{comp0} + \sum_i^I TAC_{compBlock\ i} \\
 s.t \quad & [W_{Comp0}, W_{Comp\ i}, Q_{Cooler\ i}] = f^{Implicit}(r_0, r_i, T_i) \\
 & \begin{bmatrix} Y_i \\ r^{lo} \leq r_i \leq r^{up} \\ T^{lo} \leq T_i \leq T^{up} \end{bmatrix} \vee \begin{bmatrix} \neg Y_i \\ r_i = 1 \\ T_i = T_i^{in} \end{bmatrix} \quad \forall i \in I \\
 & Y_i \Rightarrow Y_{i-1} \quad \forall i \in I \setminus \{1\} \\
 & Y_i \in \{True, False\}
 \end{aligned} \tag{4}$$

The objective function minimizes the Total Annualized Cost (TAC), which comprises the capital cost (CAPEX) and operating cost (OPEX) of the compression system (Appendix C). To determine the TAC the dependent variables (compressor powers,  $W_{Comp0}$ ,  $W_{Comp\ i}$  and cooler duty,  $Q_{Cooler\ i}$ ) are implicitly calculated at the process simulator (denoted by an implicit function,  $f^{Implicit}$ ). The stage compression selection is represented by a set of  $I$  disjunctions. If a compression block is selected ( $Y_i$ ), then the value of the design variable  $r_i$  and  $T_i$  can take any value between their lower and upper bounds. On the contrary, if the compression stage is not selected ( $\neg Y_i$ ) the compression ratio is forced to be one, and  $T_i$  is equal to the inlet cooler temperature ( $T_i^{in}$ ). Finally, a logic proposition is added to ensure that the compressor blocks are consecutive.

The GDP model (4) is reformulated as an MINLP (see Grossmann, 2002).<sup>23</sup> To do this, the disjunctions and logic proposition must be converted into algebraic forms adding binary variables. The disjunctions have been reformulated using the convex hull reformulation. The resulting MINLP is shown in Eq.(5).

$$\begin{aligned}
\min \quad & TAC_{comp0} + \sum_i^I TAC_{compBlock\ i} \\
s.t \quad & [W_{Comp0}, W_{Comp\ i}, Q_{Cooler\ i}] = f(r_0, r_i, T_i) \\
& \left. \begin{aligned}
& r_i = r_i^1 + r_i^2 \\
& y_i r_i^{lo} \leq r_i^1 \leq r_i^{up} y_i \quad r_i^2 = 1 - y_i \\
& T_i = T_i^1 + T_i^2 \\
& y_i T_i^{lo} \leq T_i^1 \leq T_i^{lo} y_i \quad T_i^2 = T_{i-1} (1 - y_i)
\end{aligned} \right\} \forall i \in I \\
& y_i \geq y_{i-1} \quad \forall i \in I \setminus \{1\} \\
& y_i \in \{0, 1\}
\end{aligned} \tag{5}$$

Finally, the equation related to the compression ratio can be reformulated as follows, because in this case  $r^{lo} = I$ :

$$r_i^{lo} \leq r_i \leq (r_i^{up} - r_i^{lo}) y_i + r_i^{lo} \tag{6}$$

The working pressure in the reactor has a high influence in overall TAC of the process. Therefore, we solve the optimization problem (4) as a function of the parameter  $P_{OUT}$ , which varies from 6000 to 8000 kPa. In overall cases, the optimal topology solution provides four compressors. Therefore, we build a correlation function between optimum TAC and  $P_{OUT}$  fixing the compression system with four stages. Then, the optimized compression system can be added to the overall DME optimization process.

$$TAC_{compression\ system} = 0.0519 \cdot P_{OUT} + 9.6292 \tag{7}$$

### 2.3 DME production

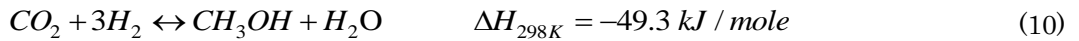
The operating conditions selected in the reactor imply that the temperature of its inlet stream should be between 220 and 300 °C. To achieve this, the resulting stream from the compressed system has to be heated or cooled.

To model this situation, we define the Boolean variables  $Y_1$  and  $Y_2$  to select a heater or a cooler, respectively.

$$\left[ \begin{array}{c} Y_1 \\ 220^\circ C \leq T^{DME, reaction} \leq 300^\circ C \\ T^{DME, in} \leq T^{DME, reaction} \end{array} \right] \vee \left[ \begin{array}{c} Y_2 \\ 220^\circ C \leq T^{DME, reaction} \leq 300^\circ C \\ T^{DME, in} \geq T^{DME, reaction} \end{array} \right] \tag{8}$$

where  $T^{DME, in}$  and  $T^{DME, reaction}$  are the temperatures entering and leaving the exchanger, respectively. To simulate the heater (E-108a), we use a heat exchanger using HP steam as a hot utility. To simulate the cooler (E-108b), we use a water-cooled heat exchanger using water as a refrigerant.

DME synthesis was modeled using a Gibbs free energy reactor. Catalyst is selected from literature.<sup>24</sup> Direct synthesis of syngas to DME comprehends the simultaneous conversion of syngas to methanol (Eqs.(9) and (10), and the dehydration of methanol (Eq.(11)):<sup>25-28</sup>



## 2.4 Product separation: sequence of distillation columns

The mix leaving the reactor is first depressurized at a pressure of 2000 kPa and cooled to 40°C before entering the separation system.

The following step in the process is the separation system. The stream leaving the cooler is sent to the separation system, where the light components (CO, H<sub>2</sub>, CO<sub>2</sub>, and CH<sub>4</sub>) and the heavy components (methanol and water) are removed, obtaining DME with the desired composition (99.95%).

To model this section, we have studied eight alternative distillation column sequences for separation of DME, light components, and heavy components (see Figure 3). We define the Boolean variables Y<sub>3</sub>, Y<sub>4</sub>, Y<sub>5</sub>, Y<sub>6</sub>, Y<sub>7</sub>, Y<sub>8</sub>, Y<sub>9</sub>, and Y<sub>10</sub> as follows:

- Direct sequence (Y<sub>3</sub>).
- Direct sequence with a thermal couple (Y<sub>4</sub>).
- Indirect sequence (Y<sub>5</sub>).
- Indirect sequence with a thermal couple (Y<sub>6</sub>).
- Prefractionator (Y<sub>7</sub>).
- Prefractionator with a thermal couple (without condenser) (Y<sub>8</sub>).
- Prefractionator with a thermal couple (without reboiler) (Y<sub>9</sub>).
- Divided Wall Column (DWC) (Y<sub>10</sub>).

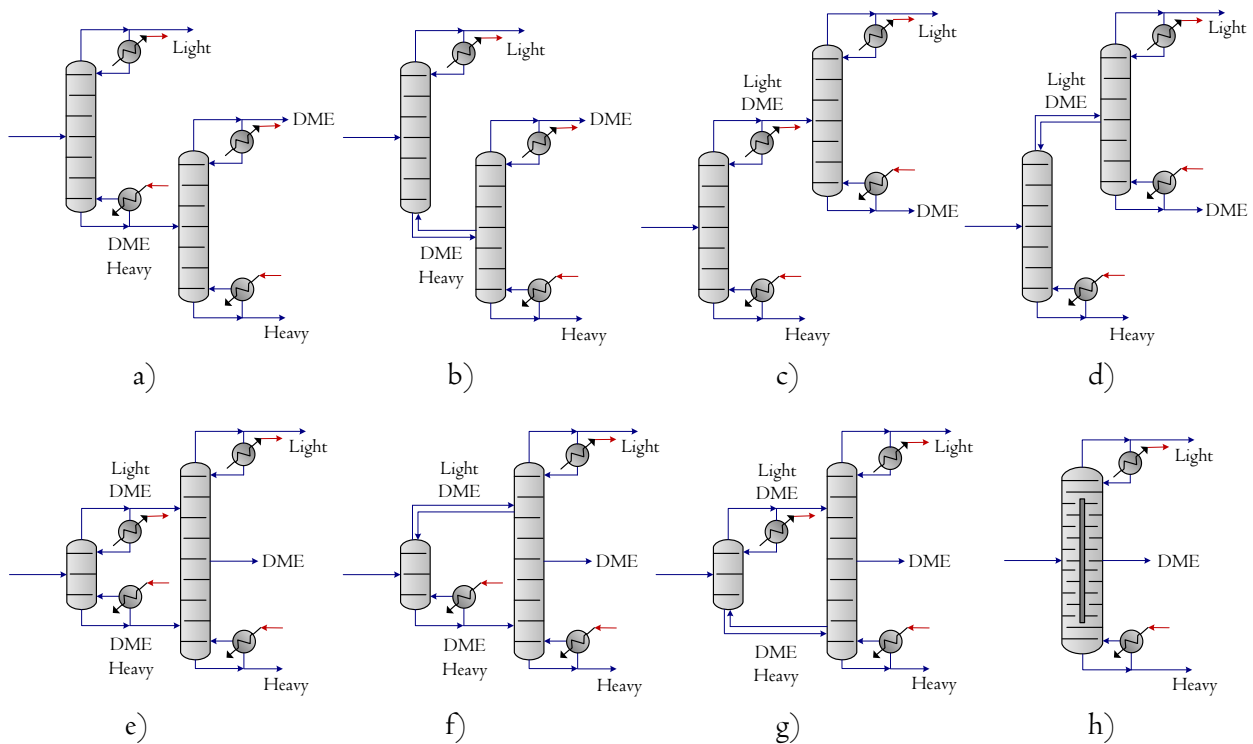


Figure 3. Eight separation configurations represented in Figure 1 as “separation sequences”.

## 3 Results and discussion

The methodology followed to develop the simulation-based optimization of the complex process superstructure is divided into the following steps (the simulation-optimization framework can be found in Appendix A). First, we build our superstructure in a chemical process simulator. The plant has been simulated on Aspen HYSYS v.8.8, and Peng-Robinson model is used as a thermodynamic package in the simulation.

The simulation-based optimization of the compression system has been performed using Aspen HYSYS. As it has been seen in the section 2.2, a correlation function between the optimum TAC and  $P_{OUT}$  has been built, in order to be added to the overall DME optimization process.

After simulating our chemical process superstructure, we performed a sensitivity analysis to identify which unit operation or set of units introduce numerical noise and/or are expensive to converge. These units are replaced by surrogate models. In this work, we focus on the Kriging interpolation<sup>29</sup> to build the surrogate models (see Appendix D). Kriging surrogate models were calibrated using MATLAB.<sup>30</sup> The distillation sequences for DME separation are slightly noisy, therefore, those units have been replaced by Kriging surrogate models. The rest of the unit operations are maintained in their original form in the process simulator.

Instead of directly reformulating our superstructure-based synthesis problem into an MINLP and solve it with the available solvers for that type of problems, we apply the Logic-Based Outer Approximation (logic-based OA) algorithm<sup>31</sup> to fully exploit the GDP representation of our problem. Thus, the underlying logic structure of the problem is retained in the model. The logic-based OA has been implemented in MATLAB and interfaced with different commercial solvers for NLP and MINLP problems through TOMLAB.<sup>32</sup> The complete model, objective function, explicit constraints, implicit models (models in the simulator) and surrogate models, are written in a proprietary language.<sup>33</sup>

The aim of this work consists of determining the best flowsheet topology to maximize the profit of the DME plant.

The objective function includes raw material costs, costs associated with utility consumptions (electricity, cooling water, refrigerant, steam, hot oil, and natural gas), annualized investment costs for equipment, and income from the sales of DME. The estimation of the capital costs are calculated using the correlations given by Turton et al.<sup>34</sup> The objective function is determined by the following expression:

$$profit = \sum_p MF_p \cdot price_p - \left( \sum_r MF_r \cdot price_r + OPEX + F \cdot CAPEX \right) \quad (12)$$

where  $MF_p$  is the mass flow of the product sold,  $price_p$  is the price of the product sold,  $MF_r$  is the mass flow of the raw materials brought,  $price_r$  is the price of the raw materials,  $OPEX$  is the operating cost per year,  $F$  is the annualization factor, and  $CAPEX$  is the capital cost of the equipment. Prices and costs have been updated by the global CEPCI cost index of 2015. The annualization factor is calculated by the equation recommended by Smith,<sup>20</sup> where we have considered a fixed interest rate of 10% and a horizon time of 8 years. The prices of the raw materials, products, and utilities are given in Table 2.

Table 2. Prices of the raw materials, products, and utilities.

Raw material/Product	Cost (\$/kg)	Utility	Cost (\$/kWh)
CO <sub>2</sub>	0.0030	Cooling water (30°C to 40°C)	0.0013
Natural gas	0.1804	Refrigerant (very low temperature -50°C)	0.0159
Water	0.0010	Electricity	0.0600
DME	0.5000	HP steam (4100 kPa, 254°C)	0.0637
		Hot oil	0.0893
		Natural gas	0.0121

The final syngas synthesis configuration includes the WGS reaction since, despite of increasing the costs, improves the H<sub>2</sub>/CO ratio, which is translated into a higher DME production. The optimal compression system consists of four stages, because fewer stages raise the compression ratio and thus the operating cost. On the other hand, more stages although further decrease the operating cost, also increase the capital cost. Finally, the best column sequence for the DME separation is obtained using a divided wall column (DWC), due to the lower energy requirements as a result of only having one condenser and one reboiler as opposed to the conventional two-column configuration. The optimal configuration is shown in Figure 4.

The maximum profit obtained is \$51.01 million/year. The main characteristics of the selected equipment in the optimal configuration are shown in Appendix C. The parameters for the Kriging surrogate models can be found in Appendix D.

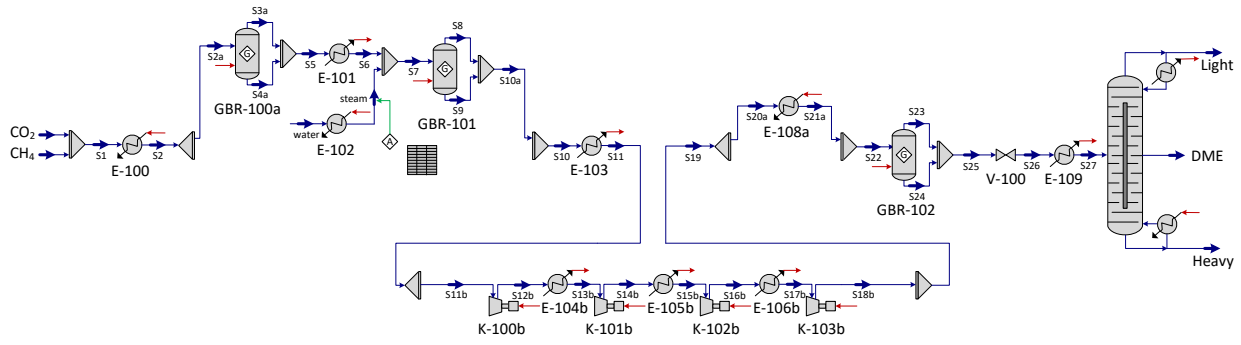


Figure 4. Optimized flowsheet for the production of DME.

### 3.1 Heat integration

Heat integration is performed to improve the energy efficiency of the DME plant. We used the Synheat MINLP model<sup>35</sup> where exchanger areas, utility cost, and selection of matches are optimized simultaneously. Figure 5 shows the HEN obtained for our plant. The data of streams involved in the heat integration are presented in Table 3. The costs of the heat integrated plant including utilities and capital cost of the HEN are \$13.68 million/year, which is 36% lower than the base case. The profit obtained after the heat integration is \$58.68 million/year.

Table 3. Data of streams involved in the heat integration.

	$T_{in}$ (°C)	$T_{out}$ (°C)	$FC_p$ (kW/°C)	Type
H1	850.00	250.00	34.16	Hot
H2	250.00	249.00	340.60	Hot
H3	250.00	40.00	31.81	Hot
H4	186.19	40.08	31.69	Hot
H5	182.87	40.05	31.78	Hot
H6	196.93	40.02	320932.00	Hot
H7	220.18	219.18	43592.77	Hot
H8	198.87	40.00	26.33	Hot
H9	-28.90	-29.90	7118.67	Hot
C1	238.94	850.00	31.67	Cold
C2	25.00	250.00	0.05	Cold
C3	849.00	850.00	68411.77	Cold
C4	192.12	220.18	32.80	Cold
C5	178.13	179.13	7043.21	Cold
C6	30.00	40.00	6248.53	Cold

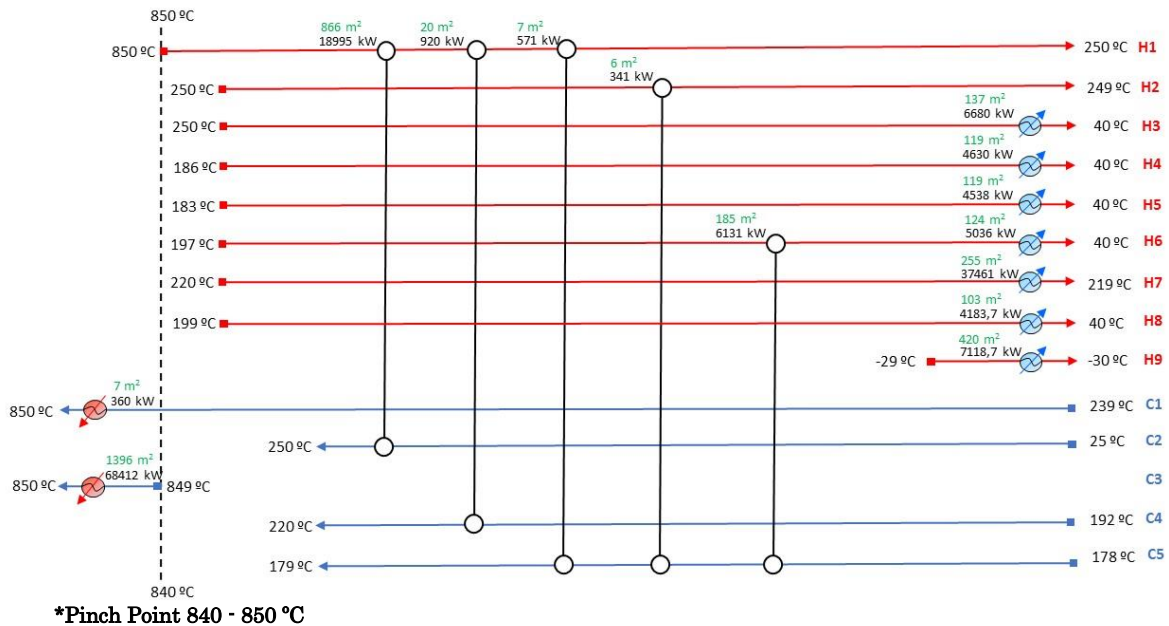


Figure 5. Heat exchanger network for the DME production.

### 3.2 Life cycle assessment (LCA)

Moreover, we evaluate the process from an environmental perspective. In particular, we have used the ReCiPe EndPoint (H,A) indicator,<sup>36</sup> available in Ecoinvent Database v.3.3.<sup>37</sup> The environmental impacts are evaluated using the principles of the Life Cycle Assessment (LCA),<sup>38</sup> which is the main instrument to evaluate the environmental performance of chemical processes.<sup>39-41</sup> First, raw materials, utilities, and processes are identified and quantified. These measures are transformed into a set of environmental impacts that are aggregated into three categories. Finally, impacts are evaluated in order to improve the process, achieving to reduce impacts.

Impacts are aggregated into seventeen categories, related to ecosystem quality, human health, and resource depletion: agricultural land occupation, climate change (ecosystems), freshwater ecotoxicity, freshwater eutrophication, marine ecotoxicity, natural land transformation, terrestrial acidification, terrestrial ecotoxicity, urban land occupation, climate change (human health), human toxicity, ionizing radiation, ozone depletion, particulate matter formation, photochemical oxidant formation, fossil fuel depletion and metal depletion.

In this work, we study impacts associated with the production of DME (the functional unit used for this calculation is the production of 1 kg of dimethyl ether).

Several studies have shown that reduction of energy consumption can accomplish the minimization of environmental impacts.<sup>42,43</sup> Therefore, impacts are calculated before and after the heat integration.

The process inventory before and after the heat integration can be found in Appendix E.

Figure 6 shows the three main categories of impact associated with each process. Clearly, impacts decrease when the heat integration is performed. Impact after heat integration is reduced by around 17% against the plant before heat integration.

The most affected category is “Resources”, basically due to the use of electricity.

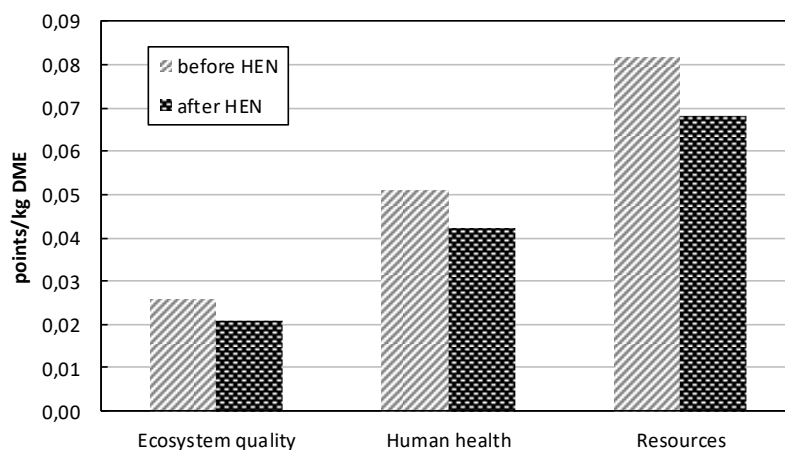


Figure 6. Main categories of impact associated with the DME process.

Finally, the LCA analysis includes both short-term and long-term perspectives. Global Warming Potential (GWP) has been calculated to show the total impact of our process before and after the heat integration. Figure 7 shows total impact associated with the process of DME production.

Net CO<sub>2</sub> emissions have been calculated in order to compare our process with the conventional process for DME production. As we can see from Figure 7, net emissions for DME production following our process are around 0.510 kg CO<sub>2</sub>-eq/ kg DME. Conventional process has an average emission of 1.321 kg CO<sub>2</sub>-eq/ kg DME. Therefore, net emissions might be reduced by 61%.

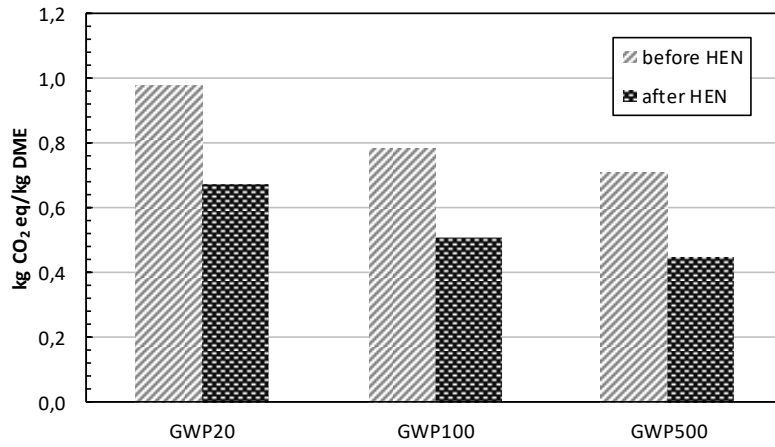


Figure 7. Short-term and long-term analysis of Global Warming Potential.

### 3.3 Safety analysis

A safety analysis of the plant was performed using Dow's Fire & Explosion Index.<sup>44</sup> Results are shown in Table 4. Individual penalties can be found in Appendix F.

Table 4. Dow's Fire & Explosion Index results

Dow's Fire & Explosion Index	
General Process Hazards Factor (F1)	1.90
Special Process Hazards Factor (F2)	4.38
Process Unit Hazards Factor (F3)	8.00
Fire and Explosion Index (F&EI)	168
Degree of Hazard	Severe
Radius of Exposure [m]	43.0

The results state that the plant possesses the highest possible explosion index assignable by the analysis (maximum of 8). However, this value is shared among other processes in which syngas is actively produced or utilized.

### 3.4 Economic feasible study

To assess the benefits from the optimal process assuming a level of uncertainty in the prices, various metrics can be employed. For our purposes, the concept of the financial risk is used.

The financial risk is a probabilistic approach to risk management defined as the probability of not meeting a certain target value,  $\Omega$ .<sup>45</sup> In the framework of the present economic study, the financial risk is referred as the probability of not meeting a desired profit with our optimal DME process. The financial risk ( $FRisk$ ) associated with our DME flowsheet,  $x$ , and a target value,  $\Omega$ , is given by Eq.(13).

$$FRisk(x, \Omega) = P[Profit(x) < \Omega] \quad (13)$$

where  $Profit(x)$  is the actual profit (the resulting profit after introducing the uncertainty). Because uncertainty in the raw material, product, and utility prices is represented by a finite number of independent scenarios, the financial risk can be defined in terms of the probability of not meeting the target value in each scenario  $s$ .

$$FRisk(x, \Omega) = \sum_{s \in S} P[Profit_s(x) < \Omega] \quad (14)$$

In addition, for each particular scenario, the profit is either greater (or equal) than the target value, in which case the probability is zero, or smaller than the target when the probability is one. Therefore, the financial risk can be expressed as Eq.(15).

$$FRisk(x, \Omega) = \sum_{s \in S} \omega_s Z_s(x, \Omega) \quad (15)$$

where  $\omega_s$  is the probability of scenario, generally taken as  $1/|S|$ , where  $|S|$  is the cardinality of the set of scenarios; and  $Z_s(\Omega)$  is a binary variable defined for each scenario (see Eq.(16)).

$$Z_s(x, \Omega) = \begin{cases} 1 & \text{if } Profit_s(x) < \Omega \\ 0 & \text{otherwise} \end{cases} \quad \forall s \in S \quad (16)$$

The profit achieved with the process is calculated through Eq.(17).

$$Profit_s(MM\$/year) = Income_s - Costs_s - TAC \quad (17)$$

Each term of Eq.(17) is given by Eq.(18).

$$\begin{aligned} Income_s(MM\$/year) &= DME Sales_s \\ Costs_s(MM\$/year) &= Natural Gas Cost_s + CO_2 Cost_s + Water Cost_s \\ TAC(MM\$/year) &= OPEX + F \cdot CAPEX \end{aligned} \quad (18)$$

A critical issue in this methodology is the generation of appropriate values of the uncertain parameters. In this work, we model the uncertainty in the raw material, product, and utility prices by a set of scenarios, generated by Monte Carlo sampling.<sup>46</sup>

There is a broad family of probability distribution functions. Some of the most common ones are the normal, uniform, triangular, and log-normal distributions. In this case, we have selected the triangular distribution for the generation of the different scenarios. This distribution is typically used in economic simulations and provides a good representation of the probability distribution for the uncertain prices when limited sample data is available.<sup>30</sup> Parameters for triangular distribution are the minimum price  $a$ , the maximum price  $b$ , and the most likely price  $c$ .

Data prices for raw materials, products, and utilities are shown in Table 5 (updated values to 2015).<sup>47</sup>

Table 5. Data prices for raw materials, products, and utilities.

Raw material	Price range (\$/kg)	Utility	Price range (\$/kWh)
CO <sub>2</sub>	0.0020 – 0.0040	Cooling water	0.0008 – 0.0018
Natural gas*	0.0903 – 0.4733	Very low temperature refrigerant	0.0100 – 0.0200
Water	0.0010	Electricity	0.0400 – 0.0800
DME	0.4000 – 1.0000	Natural gas*	0.0061 – 0.0318

\* Data obtained from [www.investing.com/commodities/natural-gas](http://www.investing.com/commodities/natural-gas), corresponding to January 1, from 1996 to 2016.<sup>48</sup>

The parameters of the triangular distribution  $a$ ,  $b$  and  $c$  are obtained from this data. The parameters  $a$  and  $b$  are obtained from Table 5, decreasing and increasing the minimum and maximum prices by 5 % respectively. And the most likely price  $c$  is estimated from the sample mean. The results are shown in Table 6.

Table 6. Triangular probability distribution model parameters.

	Natural gas (\$/kWh)	Natural gas (\$/kg)	CO <sub>2</sub> (\$/kg)	Water (\$/kWh)	Refrigerant (\$/kWh)	DME (\$/kg)	Electricity (\$/kWh)
a	0.0058	0.0858	0.0019	0.0008	0.0095	0.3800	0.0380
b	0.0334	0.4969	0.0042	0.0019	0.0210	1.0500	0.0840
c	0.0151	0.2243	0.0030	0.0013	0.0150	0.7000	0.0600

The expected value  $E[X]$ , variance  $Var[X]$  and standard deviation  $sd[X]$  of the triangular probability distribution function are obtained through the following expressions (see Table 7):

$$\begin{aligned}
E[X] &= \frac{a+b+c}{3} \\
\text{Var}[X] &= \frac{a^2+b^2+c^2-ab-ac-bc}{18} \\
\text{sd}[X] &= \sqrt{\text{Var}[X]}
\end{aligned}
\tag{19}$$

Table 7. Expected value, variance and standard deviation of the raw material and product prices.

	Natural gas (\$/kWh)	Natural gas (\$/kg)	CO <sub>2</sub> (\$/kg)	Water (\$/kWh)	Refrigerant (\$/kWh)	DME (\$/kg)	Electricity (\$/kWh)
E[X]	0.0181	0.2690	0.0030	0.0013	0.0152	0.7100	0.0607
Var[X]	0.0000	0.0073	0.0000	0.0000	0.0000	0.0187	0.0001
sd[X]	0.0057	0.0854	0.0005	0.0002	0.0023	0.1368	0.0094

The more direct way to assess the trade-offs between risk and the potential profit of the proposed DME process is to use the cumulative risk curve. For the given process, this curve shows the level of incurred financial risk at each potential profit level. Therefore, the cumulative curve is obtained when the financial risk of a set of different targets  $\Omega$  is computed and plotted. Figure 8 shows the cumulative risk curve for the optimal and heat integrated DME process for a set of expected profits ranging from 0 to 200 million dollars per year.

The curve of Figure 8 shows that the optimal profit obtained after the heat integration (\$58.68 million/year) is found for an incurred financial risk around 15.4%. In addition, as a reference value, the configuration obtained can achieve a potential profit of \$40.25 million/year with a financial risk of not achieving the target value of 5%.

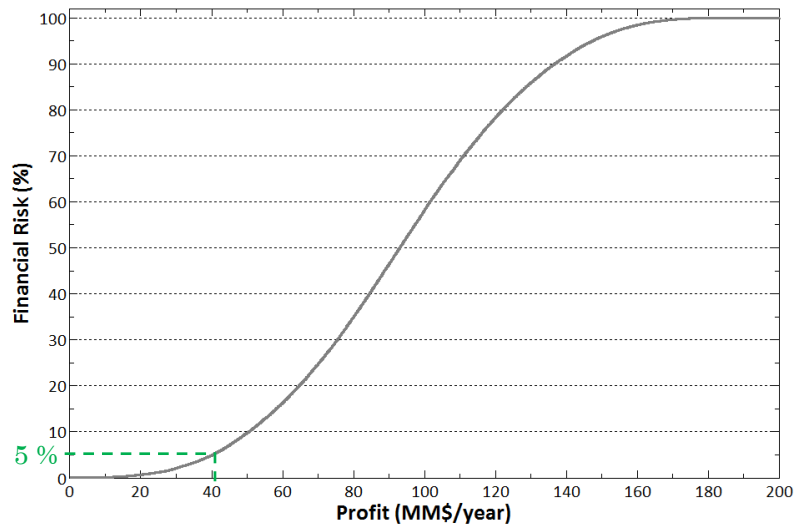


Figure 8. Cumulative risk curve.

### 3.5 Cash flow analysis

Finally, in order to study the short-term and long-term economic analysis, we have calculated the cash flow considering that the price of raw materials and DME increases by 5% each year. In Figure 9 is shown the cumulative cash flow. It remains negative during construction (the first two years) and part of the first production year. In the third year, we will start to obtain 50MM\$ of profit.

Calculations of the cash flow analysis (following the equations from Ruiz-Femenia et al., 2013)<sup>49</sup> can be found in Appendix G.

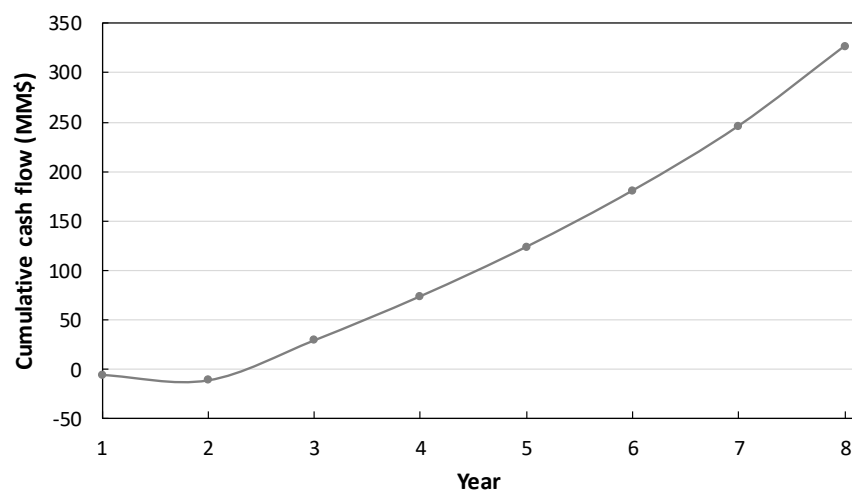


Figure 9. Cumulative risk curve.

## 4 Conclusions

Carbon capture and utilization (CCU) method is an attractive alternative to CO<sub>2</sub> storage. In this work, we propose as a case study, a dimethyl ether production process for CO<sub>2</sub> utilization that demonstrates its effectiveness and feasibility at industrial scale. Four main stages have been considered in order to build the proposed superstructure: syngas production, compression system, DME production, and product separation. The use of surrogate models in the optimization and synthesis of process flowsheets (MINLP problems) has been addressed in this work. The optimal configuration obtained can achieve a potential profit of \$51.01 million/year, emitting 0.784 kg CO<sub>2</sub>-eq/kg DME produced.

Energy integration of the process was also performed to determine the minimum utility consumption of the process, obtaining the heat exchanger network. This allows us a significant cost saving (13.1%) and the reduction of the environmental impacts (17.1%). After heat integration implementation, the profit is raised to \$58.68 million/year and emissions are reduced to 0.510 kg CO<sub>2</sub>-eq/kg DME.

The impact assessment shows that emissions are greatly reduced after comparison with the classic DME synthesis process. In addition, 122.26 kt CO<sub>2</sub>/year are consumed in the process (0.556 kg CO<sub>2</sub>/kg DME produced).

Finally, the financial risk was also studied. The financial risk of not achieving the target value (\$58.68 million/year) is around 15.4%, while the cumulative risk curve ensures around \$40.25 million/year profit with a probability of 95%.

## Appendices

---

**Appendix A:** Scheme of the modeling framework

**Appendix B:** Process flow diagram and stream data table for the optimized process

**Appendix C:** Equipment cost summary

**Appendix D:** Kriging parameters

**Appendix E:** Process inventory for impact assessment

**Appendix F:** Fire & Explosion index summary sheet

**Appendix G:** Cash flow analysis

## References

1. Aresta M, Dibenedetto A. Utilisation of CO<sub>2</sub> as a chemical feedstock: opportunities and challenges. *Dalton Trans.* 2007(28):2975-2992.
2. Aresta M, Dibenedetto A, Angelini A. The changing paradigm in CO<sub>2</sub> utilization. *J CO<sub>2</sub> Util.* 2013;3-4:65-73.
3. Elvers B. *Ullmann's Encyclopedia of Industrial Chemistry*. 6th ed. New York: John Wiley & Sons, Inc; 2002.
4. Subramani V, Gangwal SK. A review of recent literature to search for an efficient catalytic process for the conversion of syngas to ethanol. *Energy Fuels.* 2008;22(2):814-839.
5. Song Y, Peng R, Hensley DK, et al. High-Selectivity Electrochemical Conversion of CO<sub>2</sub> to Ethanol using a Copper Nanoparticle/N-Doped Graphene Electrode. *Chemistry Select.* 2016;1(19):6055-6061.
6. Bobrova LN, Bobin AS, Mezentsseva NV, Sadykov VA, Thybaut JW, Marin GB. Kinetic assessment of dry reforming of methane on Pt+Ni containing composite of fluorite-like structure. *Appl Catal B: Environ.* 2016;182:513-524.
7. Kim YH. Rigorous design of extended fully thermally coupled distillation columns. *Chem Eng J.* 2002;89(1-3):89-99.
8. Li Z, Feng J, Yan S, Zou Z. Solar fuel production: Strategies and new opportunities with nanostructures. *Nano Today.* 2015;10(4):468-486.
9. Yuan L, Xu Y-J. Photocatalytic conversion of CO<sub>2</sub> into value-added and renewable fuels. *Appl Surf Sci.* 2015;342:154-167.
10. Kurtz BE. Homogeneous kinetics of methyl chloride chlorination. *Ind Eng Chem Res.* 1972;11(3):332-338.
11. Azizi Z, Rezaeimaneh M, Tohidian T, Rahimpour MR. Dimethyl ether: A review of technologies and production challenges. *Chem Eng Process.* 2014;82:150-172.
12. Duraccio V, Gnoni MG, Elia V. Carbon capture and reuse in an industrial district: A technical and economic feasibility study. *Journal of CO<sub>2</sub> Utilization.* 2015;10:23-29.
13. Nuchitprasittichai A, Cremaschi S. Optimization of CO<sub>2</sub> capture process with aqueous amines using response surface methodology. *Computers & Chemical Engineering.* 2011;35(8):1521-1531.
14. Zahedi nezhad M, Rowshanzamir S, Eikani MH. Autothermal reforming of methane to synthesis gas: Modeling and simulation. *Int J Hydrogen Energy.* 2009;34(3):1292-1300.
15. Froment GF. Production of synthesis gas by steam- and CO<sub>2</sub>-reforming of natural gas. *J Molec Catal A-Chem.* 2000;163(1-2):147-156.
16. Song C. Tri-reforming: A new process concept for effective conversion and utilization of CO<sub>2</sub> in flue gas from electric power plants. *ACS Fuel Chemistry.* 2000;45(4):772-776.
17. Song X, Guo Z. Technologies for direct production of flexible H<sub>2</sub>/CO synthesis gas. *Energ Convers Manage.* 2006;47(5):560-569.
18. Weissman M, Benson SW. Pyrolysis of methyl chloride, a pathway in the chlorine-catalyzed polymerization of methane. *Int J Chem Kinet.* 1984;16(4):307-333.
19. Schakel W, Oreggioni G, Singh B, Strømman A, Ramírez A. Assessing the techno-environmental performance of CO<sub>2</sub> utilization via dry reforming of methane for the production of dimethyl ether. *J CO<sub>2</sub> Util.* 2016;16:138-149.
20. Smith R. *Chemical process: Design and integration*. Chichester: John Wiley & Sons; 2005.
21. Balas E. Disjunctive Programming. In: Hammer PL, Johnson EL, Korte BH, eds. *Annals of Discrete Mathematics*. Vol 5. Canada: Elsevier; 1979:3-51.
22. Raman R, Grossmann IE. Modelling and computational techniques for logic based integer programming. *Comput Chem Eng.* 1994;18(7):563-578.
23. Grossmann IE. Review of Nonlinear Mixed-Integer and Disjunctive Programming Techniques. *Optim Eng.* 2002;3(3):227-252.
24. Lebarbier VM, Dagle RA, Kovarik L, Lizarazo-Adarme JA, King DL, Palo DR. Synthesis of methanol and dimethyl ether from syngas over Pd/ZnO/Al<sub>2</sub>O<sub>3</sub> catalysts. *Catal Sci Technol.* 2012;2(10):2116-2127.
25. Lee S, Sardesai A. Liquid phase methanol and dimethyl ether synthesis from syngas. *Top Catal.* 2005;32(3):197-207.
26. Moncada J, Posada JA, Ramírez A. Early sustainability assessment for potential configurations of integrated biorefineries. Screening of bio-based derivatives from platform chemicals. *Biofuels, Bioproducts and Biorefining.* 2015;9(6):722-748.
27. Moradi F, Kazemeini M, Fattahi M. A three dimensional CFD simulation and optimization of direct DME synthesis in a fixed bed reactor. *Petrol Sci.* 2014;11(2):323-330.
28. Papari S, Kazemeini M, Fattahi M. Modelling-based Optimisation of the Direct Synthesis of Dimethyl Ether from Syngas in a Commercial Slurry Reactor. *Chinese J Chem Eng.* 2013;21(6):611-621.
29. Krige DG. *A statistical approach to some mine valuation and allied problems on the Witwatersrand*. [Master's thesis]. South Africa: University of Witwatersrand 1951.
30. *The Mathworks, Inc. Matlab 8.3* [computer program]. Natick, MA: The Mathworks, Inc; 2014.
31. Turkyay M, Grossmann IE. Logic-based MINLP algorithms for the optimal synthesis of process networks. *Comput Chem Eng.* 1996;20(8):959-978.
32. Holmström K. The TOMLAB optimization environment in Matlab. *Adv Model Optim.* 1999;1(1):47-69.
33. Caballero JA, Navarro MA, Ruiz-Femenia R, Grossmann IE. Integration of different models in the design of chemical processes: Application to the design of a power plant. *Appl Energy.* 2014;124:256-273.
34. Turton R, Bailie RC, Whiting WB, Shaeiwitz JA. *Analysis, synthesis, and design of chemical processes*. 4th ed. Upper Saddle River, New Jersey: Prentice Hall; 2013.

35. Yee TF, Grossmann IE. Simultaneous optimization models for heat integration II. Heat exchanger network synthesis. *Comput Chem Eng.* 1990;14(10):1165-1184.
36. Goedkoop M, Heijungs R, Huijbregts M, Schryver AD, Struijs J, Van Zelm R. *ReCiPe 2008. A life cycle impact assessment method which comprises harmonised category indicators at the midpoint and the endpoint level.* 2013.
37. Weidema BP, Bauer C, Hischer R, et al. *Data quality guideline for the ecoinvent database version 3. Overview and methodology.* Swiss Centre for Life Cycle Inventories 2013.
38. Guinée JB, Gorrée M, Heijungs R, et al. *Handbook of Life Cycle Assessment. Operational guide to the ISO Standards.* Dordrecht: Kluwer Academic Publishers 2002.
39. Azapagic A, Clift R. The application of life cycle assessment to process optimisation. *Comput Chem Eng.* 1999;23(10):1509-1526.
40. Hoffmann VH, Hungerbühler K, McRae GJ. Multiobjective screening and evaluation of chemical process technologies. *Ind Eng Chem Res.* 2001;40(21):4513-4524.
41. Petrie BA, Romagnoli J. Process synthesis and optimisation tools for environmental design: methodology and structure. *Comput Chem Eng.* 2000;24(2-7):1195-1200.
42. Lara Y, Lisboa P, Martínez A, Romeo LM. Design and analysis of heat exchanger networks for integrated Ca-looping systems. *Appl Energy.* 2013;111:690-700.
43. Morar M, Agachi PS. Review: Important contributions in development and improvement of the heat integration techniques. *Comput Chem Eng.* 2010;34(8):1171-1179.
44. *Dow's Fire & Explosion Index Hazard Classification Guide.* 7th ed: American Institute of Chemical Engineers; 1994.
45. Barbaro A, Bagajewicz MJ. Managing financial risk in planning under uncertainty. *AIChE J.* 2004;50(5):963-989.
46. Marsaglia G, Tsang WW. The ziggurat method for generating random variables. *J Stat Softw.* 2000;5(8):1-7.
47. ICIS. ICIS: Indicative Chemical Prices 2015; <http://www.icis.com/chemicals/channel-info-chemicals-a-z/>. Accessed 2016 Jul.
48. Investing. [www.investment.com/commodities/natural-gas](http://www.investment.com/commodities/natural-gas). Accessed 2016 Dec.
49. Ruiz-Femenia R, Guillén-Gosálbez G, Jiménez L, Caballero JA. Multi-objective optimization of environmentally conscious chemical supply chains under demand uncertainty. *Chem Eng Sci.* 2013;95:1-11.